Synthesis and Characterization of Silicon and Nitrogen Containing Carbon-Based Crystals and Their Nanostructured Materials

Hui Lin Chang,[a,b,z] Chi Tso Chang,[a] and Cheng Tzu. Kuo[a]

[a]*National Chiao Tung University, Department of Material Science and Engineering, HsinChu, Taiwan*
[b]*Process Development Team (2PJT), Semiconductor R & D Center, Samsung Electronics, Korea*

The synthesis of carbon-based materials, such as man-made diamonds, superhard C_3N_4 materials, SiCN crystals, and other carbon-based nanostructured materials, has attracted considerable attention for many decades in academic and industrial communities. However, so far, researchers have not successfully linked the growth mechanisms of carbon-based materials deposited under different synthetic conditions and methods. In fact, a single machine may produce many of these materials. This paper is aimed to study the linkages among various carbon-based materials synthesized on Si wafers using the same microwave plasma chemical vapor deposition system, including SiCN crystalline films, SiCN nanotubes, carbon nanotubes (CNTs), conical carbon nanorods, and other nanostructured materials.
 [DOI: 10.1149/2.0181410jss]

Manuscript submitted July 3, 2014; revised manuscript received July 28, 2014. Published August 21, 2014.

Sustaining Moore's law requires constant transistor scaling, boosting the creation of new materials for future nanoelectronics applications. Several emerging materials, such as Si nanowires, carbon nanotubes (CNTs), and III–V semiconductor field effect transistors (FETs), are potential components in this continuous shrinking process. In particular, CNTs are expected to overcome the physical limitation of current Si transistors and Cu interconnections in molecular electronics.[1–5] However, their integration into Si-based metal-oxide-semiconductor field effect transistors (MOSFETs) or new nanoelectronics remains challenging when developing these transistors and interconnections. They are naturally deposited as bundles in a vertical direction because they tend to adhere to each other vertically. Vertically aligned nanotube field-effect transistors (VCNTFETs) have been proposed to yield the Si device characteristics required for 2016, as set by the International Technology Roadmap for Semiconductors.[6–12] The feasibility of this vision depends on direct approaches to achieve selective depositions in the trenches or holes of Si wafers. The deposition of CNTs bundles in the trenches and holes as channels and conductors, respectively, can provide sufficient current density. The manipulation of CNTs orientation in either horizontal or vertical direction also plays a key role in manufacturing. This study systematically evaluates the synthesis of CNTs by microwave plasma chemical vapor deposition (MPCVD) using an Fe catalyst, a $CoSi_2$ film, and Ni islands, which frequently serve as gate electrodes and contact materials in Si microelectronics. The selective growth of CNTs in trench/hole/planar forms is also examined in conjunction with their morphology and nanostructures. The field emission characteristics of CNTs deposited in trenches and holes are examined to determine electronic performance. Moreover, the electronics properties of nanocrystals and tubular structures are compared. The growth mechanism and electronic properties of nanostructured materials are addressed.

Experimental

Figure 1 schematically shows relative positions between plasma and sample in a MPCVD system. Figure 2 compares various carbon-based materials synthesized on Si wafers using the same MPCVD system. Process parameters are divided into three groups, i.e., nanotubes, nanowires, and nanocrystals, according to the synthesized material structures. Main parameters include temperature, reactive gas type (CH_4/H_2, CH_4/N_2, $CH_4/H_2/N_2$), catalyst (Fe, Co Ni), additional Si source, and patterning design for selective CNTs growth. Deposition temperatures are estimated by placing a thermocouple under a substrate holder. Nanotube morphologies and microstructures were identified by scanning (SEM) and transmission (TEM) electron microscopes. Field emission properties were evaluated by I-V measurements at 10^{-6} Torr for electrode separations of 50 and 100 μm. Table I lists the detail parameters of each sample and its corresponding morphology.

Results and Discussion

Nanostructured material synthesis by MPCVD.— Figure 2 shows the linkages among various carbon-based materials synthesized on Si wafers using the same MPCVD system at different parameters, such as temperature, gas types (CH_4/H_2, N_2), deposited buffer layer (Co and Ti),[13] additional Si source, and pattern design for selective CNTs growth. Three routes (①, ② and ③ in Fig. 2) were compared for the catalyst-assisted synthesis of carbon nanowires and nanorods as well as selective CNTs growth. The results reveal that formation and properties of CNTs can be manipulated by applying catalysts with H_2 reduction gas (CH_4/H_2 ratio = 10 sccm /100 sccm, temperature at 500°C) leading to CNTs formation (Fig. 3). In contrast, Condition 2 (route ② in Fig. 2) is under lower CH_4/H_2 ratio (CH_4/H_2 ratio = 1 sccm /100 sccm, temperature at 450°C) leading to nanowire formation. (Fig. 4). The CH_4/H_2 ratio influences the formation of tubular and crystalline structures. A high CH_4/H_2 ratio favors the formation of C-sp^2 bonding (graphite structure), whereas, a low CH_4/H_2 ratio favors the formation of C-sp^3 bonding (diamond structure). Therefore, carbon atoms surround the catalysts and later precipitate from them with different CH_4/H_2 ratios to form hollow tubes or solid nano-wires. Under Condition 3 (route ③ in Fig. 2), CNTs were selectively deposited on patterned wafers, such as (a) parallel Fe-coated line arrays and (b) $CoSi_x$-coated hole arrays. This novel method is compatible with Si microelectronic device manufacturing, as shown in Figs. 5 and 6. In addition, Fig. 5b shows 18 μm-long CNTs selectively deposited on Fe-coated line arrays at 3 μm/min. These CNTs are essentially well aligned, uniform in size, and perpendicular to the substrate. Fig. 6 shows that CNTs are also selectively deposited in the holes of Si wafers patterned with hole arrays (aspect ratio 6). SEM micrographs reveal the 5 nm-diameter CNTs are wrapped inside the holes rather than forming well-aligned CNTs (Fig. 5) under similar conditions, suggesting the high selectivity of this process. The wrapping of the CNTs in the holes may result from the local circular flow of gases in each hole.

To summarize, nanostructured carbon nanowires and nanorods were successfully synthesized on patterned and unpatterned Si wafers in the presence of a catalyst by varying the process parameters, such as catalyst materials, source gases, gas ratios, and deposition temperatures. This result also offers a different perspective on the mechanism of the catalyst-assisted MWCNTs growth. The CH_4/H_2 ratio influences the formation of tubular and crystalline structures. Specifically,

[z]E-mail: huilinchang@fas.harvard.edu

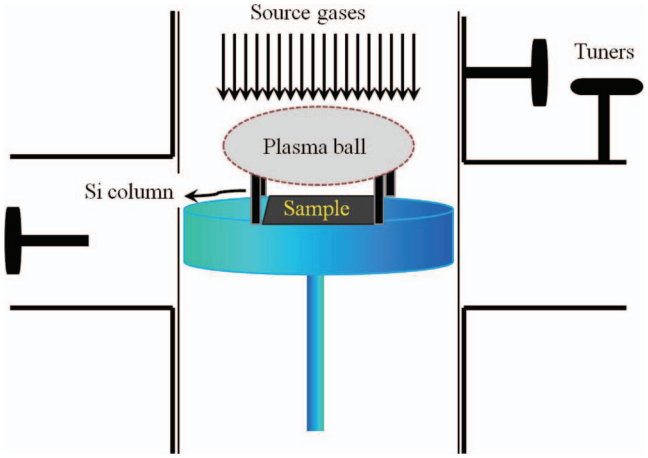

Figure 1. Relative positions between plasma and the sample in a reactor.

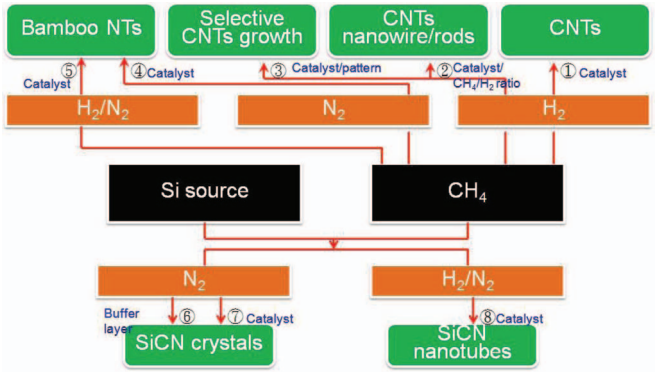

Figure 2. Process roadmaps of forming various carbon based materials.

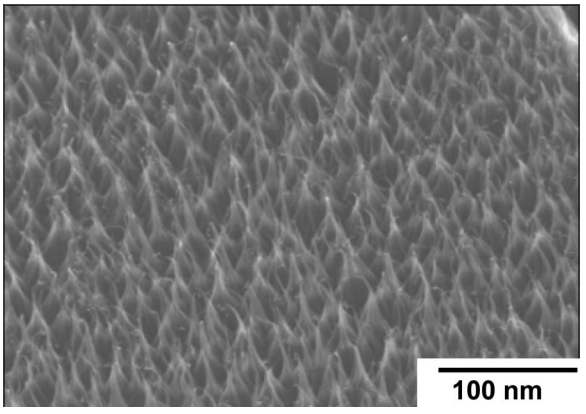

Figure 3. Orientated CNTs formation under condition 1 by applying catalysts with H_2 reduction gas (CH_4/H_2 ratio = 10 sccm /100 sccm, temperature at 500°C).

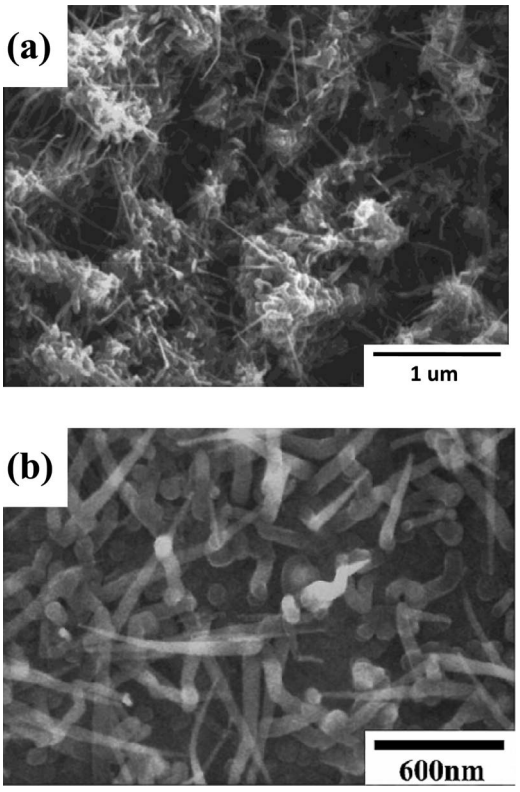

Figure 4. Nanowire formation under condition 2 by applying catalysts with H_2 reduction gas (CH_4/H_2 ratio = 1sccm /100 sccm, temperature at 450 °C). (a) Catalyst assisted nanowire formation (b) Catalyst assisted nanorodformation.

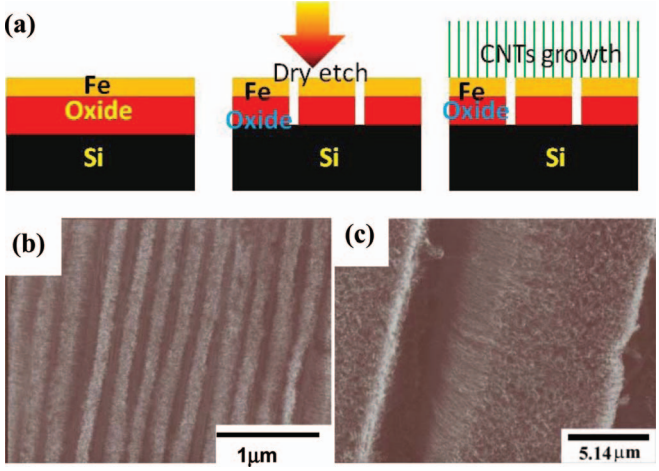

Figure 5. Process flows of forming CNTs on Fe trench arrays, oxide film deposition → Fe film deposition → dry etching → CNTs growth Fe assisted CNTs deposition on trench array in low and high magnification. Fe assisted CNTs deposition (b) trench arrays (c) high magnification.

TABLE I. Sample designations and conditions.

Route	Catalyst	Source gases (sccm/sccm/sccm)	Additional Si source	Plasma power, (W)	Morphology
①	Fe, Co, Ni	CH_4/H_2 = 10/100	No	500 ∼900	nanotubes
②	Fe, Co, Ni	CH_4/H_2 = 1/100	No	500∼900	Nanowire/nanorodes
③	Fe, Co	CH_4/H_2 = 10/100	No	500∼900	Selective nanotubes growth
④	Fe, Co, Ni	CH_4/N_2 = 10/100	No	500∼900	Bamboo nanotubes
⑤	Fe, Co, Ni	$CH_4/N_2/H_2$ = 10/100/100	No	500∼900	Bamboo nanotubes
⑥	–	CH_4/N_2 = 10/100	Yes	500∼900	Crystals
⑦	Co	CH_4/N_2 = 10/100	Yes	500∼900	Crystals
⑧	Fe	$CH_4/N_2/H_2$ = 10/100/100	Yes	500∼900	SiCN nanotubes

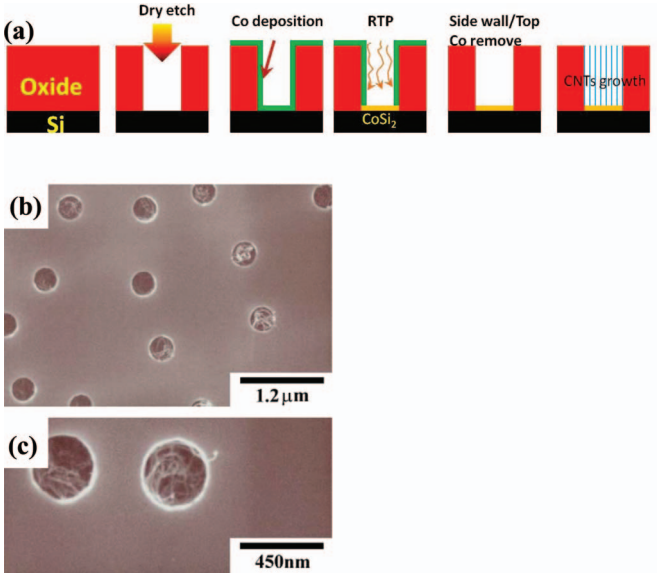

Figure 6. (a) Process flows of forming CNTs on $CoSi_2$ holes, oxide film deposition → dry etching → Co film deposition → RTP ($CoSi_2$ formation)→ unreacted metal removal → CNTs growth. $CoSi_2$ assisted CNTs deposited in holes in low and high magnification. $CoSi_2$ assisted CNTs (b) deposited in hole arrays(c) high magnification.

this CH_4/H_2 ratio promotes C-sp^2 bonding (graphite structure) when high but C-sp^3 bonding when low (diamond structure). Therefore, carbon atoms surround the catalysts and later precipitate from them to form hollow tubes or solid nanorods at different CH_4/H_2 ratios.

In addition, Conditions 4 and 5 (route ④ in Fig. 2) demonstrate the importance of nitrogen in bamboo NT formation. In the previous studies, bamboo-like nanotubes using different catalysts, such as Fe, Ni, or Ni: Cu: Al alloy can be produced in many ways, including arc discharge,[14] microwave plasma CVD[15] and thermal pyrolysis methods.[16] Therefore, formation of bamboo-like structures seems to be independent of the deposition method and catalyst type. The proposed formation mechanisms of bamboo structures, including open-ended growth[17] and stress-induced catalyst jumping,[18] seem unable to explain the results presented here. We propose the nitrogen plasma exhibits greater bombardment energy than hydrogen plasma because of larger atomic size of nitrogen compared to hydrogen. Therefore, the presence of nitrogen during CNTs growth keeps the upper catalyst surface clean and active to prolong surface passivation and enhance carbon bulk diffusion. In our previous study, we adopted a series of treatments including H_2, NH_3 and N_2 treatment and concluded nitrogen based treatment can lead to nanoparticle agglomeration.[19] A higher bombardment energy of nitrogen plasma facilitates agglomeration effects during catalyst pretreatment and initial CNTs growth stages, producing larger size nanoparticles. On the other hand, introducing N atoms into the carbon nanotube structure may induce distortion by changing its bonding to pentagonal, heptagonal, or other crystal lattices and increasing bending stress. Fig. 7 shows the bamboo NT TEM image and its corresponding SEM morphology.

Conditions 6 and 7 (route ⑥ in Fig. 2) show that appropriate timing of an additional solid source, such as Co-coated Si columns, can be used to vary SiCN film compositions, morphologies, structures, and properties[20] By comparing the conditions of forming catalyst-assisted SiCN nanotubes without forming SiCN films (Condition 8, route ⑧), Figure 8 shows the growth models of SiCN crystals formation and SiCN nanotubes formation. Figures 9a and 9b show SEM images of crystalline SiCN and tubular SiCN, respectively. The tubular SiCN electron energy loss spectroscopy (EELS) spectrum and its corresponding X-ray photoelectron spectroscopy (XPS) spectrum are shown in Fig. 10. Growth models for SiCN crystals and nanotubes suggest that additional solid Si sources are the main silicon contribu-

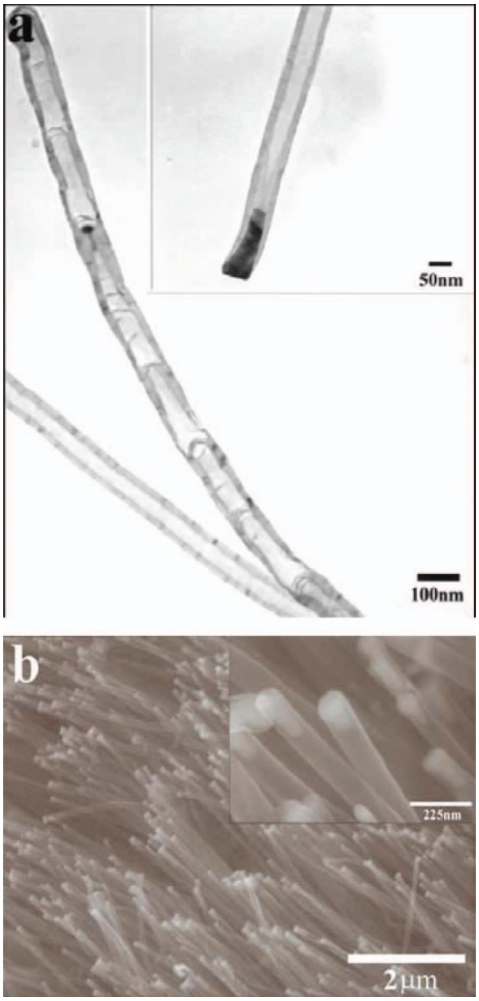

Figure 7. The formation of bamboo-like CNTs includes the presence of nitrogen and keeping an active and clean top surface of the catalyst particles. (a) TEM image of bamboo-like CNTs (b) SEM morphology.

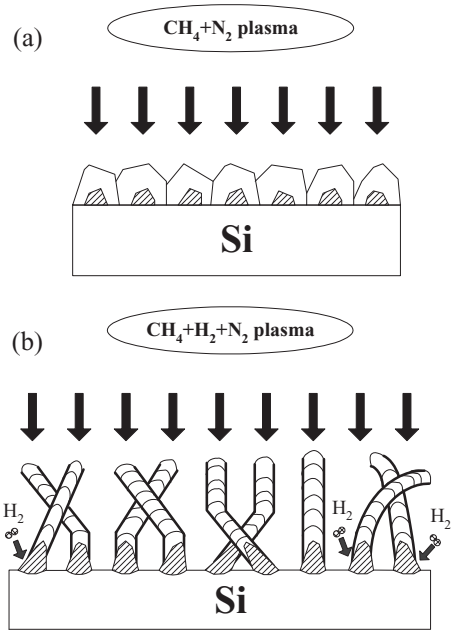

Figure 8. Growth models of (a) SiCN crystals (b) SiCN nanotubes, the shaded particle indicates the catalysts.

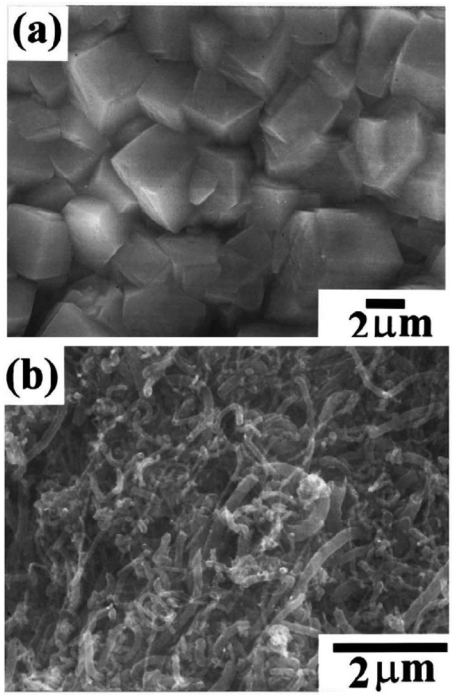

Figure 9. SEM morphologies of (a) SiCN crystals and (b) SiCN nanotubes formed using Co catalyst film.

tors to SiCN crystals and nanotubes. The tubular structure may stem from the introduction of H_2 gas during the deposition, which may delay the so-called catalyst poisoning and keep the tube end open during growth. Although some Si could be derived from the Si substrate, the plasma ionized solid Si columns actively participate in the reaction. The nano-sized catalysts promote the formation of tubular, wire, or rod morphologies. Catalytic functions in the H_2-free process differ from those in the presence of H_2 gas. Catalysts have been proposed to provide nucleation sites for SiCN crystal nucleation and effectively reduce the energy of formation during the initial stages. This catalytic function is lost when the growing film covers the catalytic particle. In contrast, the role of the catalyst during SiCN tube formation is similar to that described in the vapor–liquid–solid mode.[21] The tube grows by precipitating of graphite sheets from a supersaturated catalytic droplet. The formation of a curved graphite basal plane is energetically favorable, giving rise to a tubular structure.

Horizontal and vertical CNTs growth.— The preferred growth orientation of CNTs was examined in detail. Field alignment using applied direct current bias (−200 V) can direct CNTs growth perpendicularly to the substrate (Fig. 11). Moreover, the catalyst density is also important in determining CNTs growth direction. Many vertically grown, dense MWCNTs are found to protrude from a single catalyst particle, which may be associated with the lower temperatures during H_2-mediated reduction and CNTs deposition stages. Gaseous sources also play crucial role in controlling CNTs growth orientations. When the flow gas is guided horizontally with respect to the substrate, CNTs grow in the same direction. Two catalysts plates produce horizontal CNTs growth while separate catalyst islands leads to horizontal CNTs formation. The CNTs are deposited horizontally between splitting catalyst islands. (Fig. 12).

Electronic behaviors of nanostructured materials.— The current density–electric field (J–E) curves of SiCN crystals and tubes are compared in Fig. 13. Nanotubes $\alpha\nu\delta$ crystals show a turn-on electric field ($E_{turn\text{-}on}$) of 2 and 2.5 V/μm, respectively, at J = 1μA/cm, indicating that nanotubes display better field emission properties than crystals. According to the Fowler–Nordheim equation, the relation-

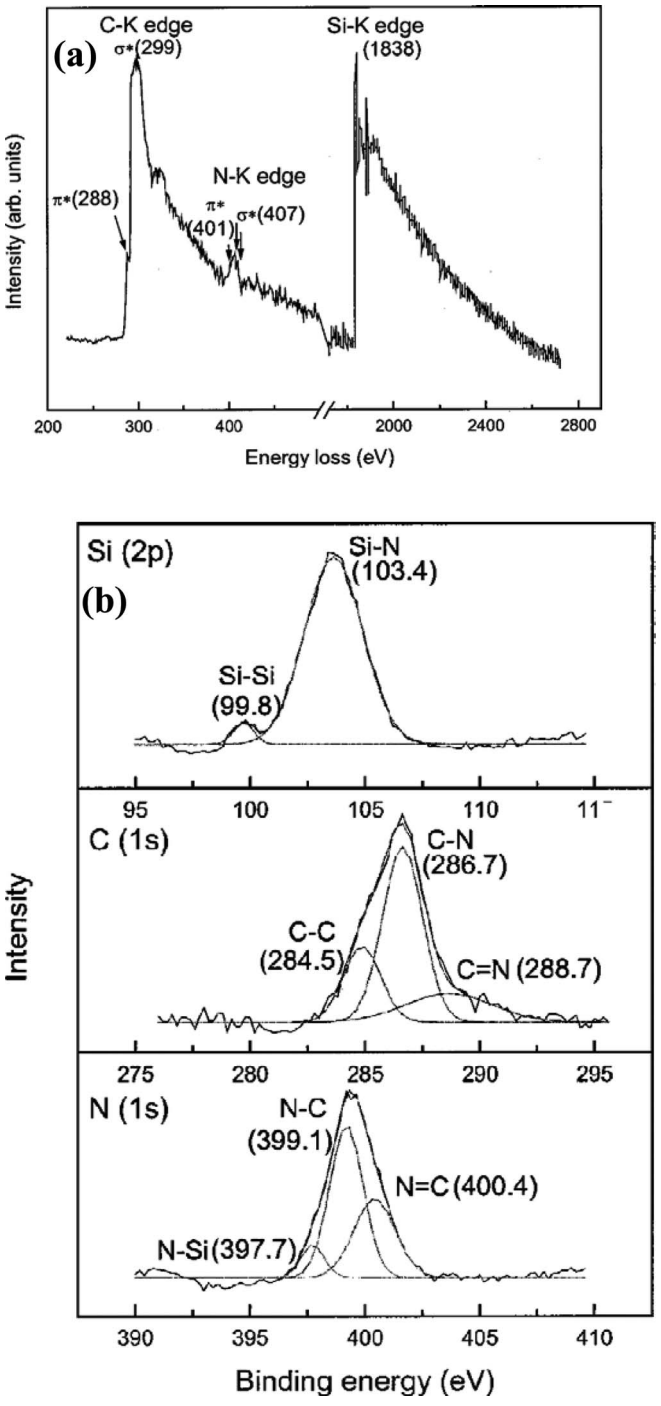

Figure 10. (a) EELS spectrum of SiCN nanotube recorded from the tube walls. (b) The corresponding XPS spectrum of SiCN crystals Si(2*p*) core level, C (1*s*) core level, and N (1*s*) core level.

ship between current (I) and applied voltage (V) can be expressed as follows:[22]

$$I = aV^2 \exp\left(\frac{-b}{V}\right)$$

$$a = \frac{\alpha A \beta^2}{1.1\phi} \exp\left[\frac{\beta(1.44 \times 10^{-7})}{\phi^{1/2}}\right]$$

$$b = \frac{0.95B\phi^{3/2}}{\beta}$$

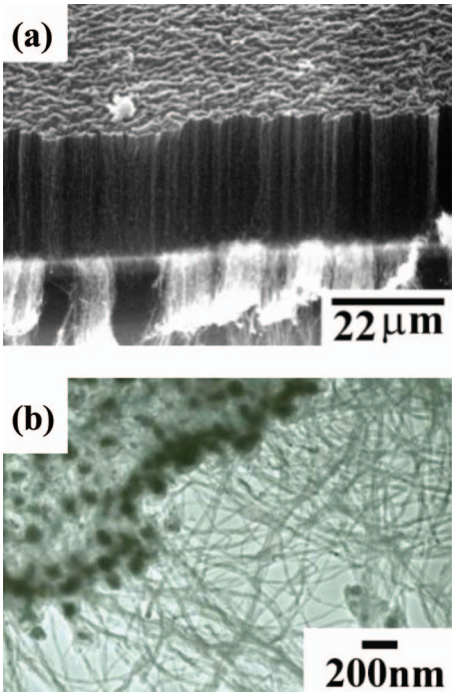

Figure 11. (a) Vertically grown CNTs (DC bias -200V) and (b) their corresponding TEM.

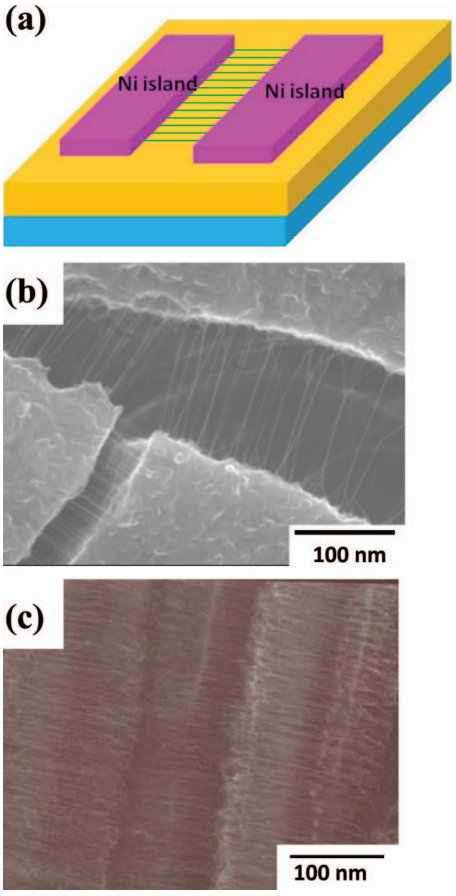

Figure 12. (a) Schematic diagram of horizontal CNTs growth on parallel Ni islands. (b), (c) Corresponding SEM images of horizontal CNTs growth in between two islands.

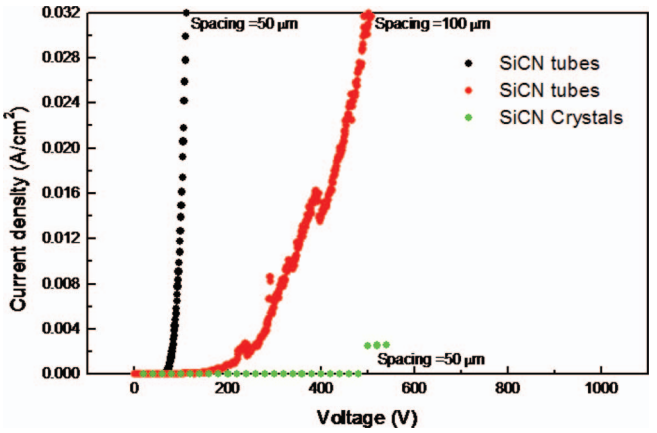

Figure 13. J-E curves of SiCN tubes and SiCN crystals. The corresponding current density of 1mA/cm^2 is obtained at 2.56 and 7.98V/μm.

Where A and B are constants (A = 1.54 × 10^{-6}, B = 6.87 × 10^7), Φ is the work function, α is the effective emitting area, and β is the field enhancement factor. Threshold voltage and emission current strongly depend on the work function of the material, effective emitting area, and field enhancement factor, which is related to the microstructure sharpness. Therefore, SiCN nanotubes present a lower threshold voltage than the nanocrystals because of their higher field enhancement factor. Figure 14 compares J–E curves obtained using Fe assisted CNTs at trenches and $CoSi_2$ assisted CNTs at holes. At a current density of 1μm/cm^2, turn-on electrical fields are obtained at 2.71 and 4.03 V/μm for CNTs in trenches and holes, respectively. Alternatively, a corresponding current density of 1 mA/cm^2 is obtained at 3.97 and 6.30 V/μm for CNTs in trenches and holes, respectively. The low turn-on electrical field of the CNTs at high current density indicates a robust electrical performance. Figure 15 compares the J-E curves obtained from horizontal CNTs and vertical CNTs. The electrical fields at a current density of 1mA/cm^2 are 1.57 and 4.32 V/μm for CNTs in horizontal and vertical to substrate direction, respectively. The horizontal CNTs show better field emission property than vertical CNTs. This may be due to the fact that the field emission of the vertical CNTs is more restricted by the catalysts at the tips and their effective emission area from defects of the CNTs body is effectively diminished by the neighboring CNTs. The CNTs body size, which can contribute to field emission, is greater in horizontal CNTs in comparison to vertical CNTs. Given that the latter are restricted by neighboring CNTs, their effective area for field emission is rather limited.

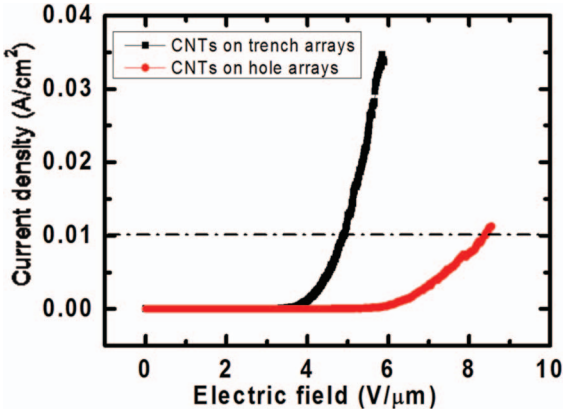

Figure 14. J-E curves of CNTs at trenches and holes. The corresponding current density of 1mA/cm^2 is obtained at 3.97 and 6.30 V/μm.

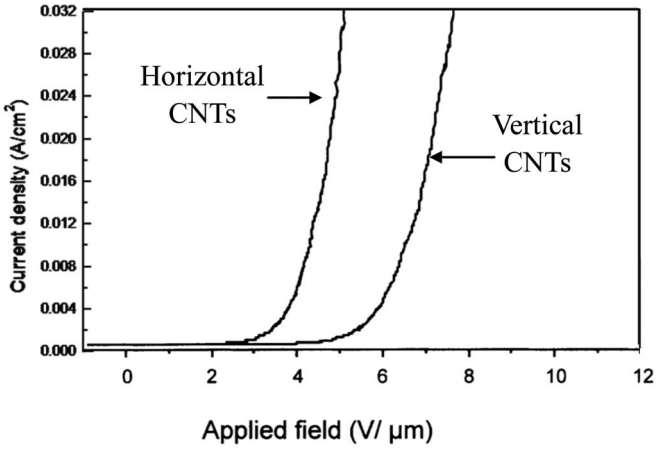

Figure 15. J-E curves of CNTs with preference orientation horizontal and vertical to the substrate. The corresponding current density of 1mA/cm^2 is obtained at 1.57 and 4.32 V/μm, respectively.

Conclusions

On account of Moore's law which relies on constant transistor scaling, emerging materials such as Si nanowires, carbon nanotubes, and III–V semiconductor FETs, are expected to transform future nanoelectronics applications validating this theory. This study demonstrates selective CNTs deposition methods that lead to vertically and horizontally oriented growth. In addition, several SiCN and carbon-based nanostructures are successfully synthesized using the same MPCVD system. The development of nanostructured materials with unique electrical properties may expand nanoelectronic device applications.

Acknowledgments

The authors thank the National Science Council of the Republic of China, Taiwan for financially supporting this research. The authors also thank Dr. M. S. Liang, Dr. E. S. Jung and Dr. J. H. Ku, Dr. M. C. Kim and Dr. B. Y. Ku for their valuable discussion.

References

1. V. V. Mitin, V. A. Kochelap, and M. A. Stroscio, *Introduction to nanoelectronics* (Cambridge, 2008), p10.
2. S. Iijima, *Nature (Lond.)* **354**, 56 (1991).
3. T. W. Ebbseen, H. J. Lezec, H. Hiura, J. W. Bennett, H. F. Ghaemi, and T. Thio, *Nature* **382**, 54 (1996).
4. W. A. de Heer, W. A. Chatelain, and D. A. Ugarte, *Science* **270**, 1179 (1995).
5. G. S. Duesberg, A. P. Graham, F. Kreupl, M. Liebau, R. Seidel, E. Unger, and W. Hoenlein, *Dia. Relat. Mar.* **13**, 354 (2004).
6. B. Q. Wei, R. Vajtai, and P. M. Ajayan, *Appl. Phys. Lett.* **79**, 1172 (2001).
7. P. Avouris, *Acc. Chem. Res.* **35**, 1026 (2002).
8. V. Derycke, R. Martel, J. Appenzeller, and P. Avouris, *Nano Lett.* **1**, 453 (2001).
9. J. Chaste, L. Lechner, P. Morfin, G. Fve, T. Kontos, J. M. Berrorir, D. C. Glattli, H. Happy, P. Hakonen, and B. Plaais, *Nano Lett.* **8**, 525 (2009).
10. R. V. Seidel, A. P. Graham, J. Kretz, B. Rajasekharan, G. S. Duesberg, M. Liebau, E. Unger, F. Kreuppl, and W. Hoenlein, *Nano Lett.* **5**, 147 (2005).
11. Sander J. Tans, Alwin R. M. Verchueren, and Cees Dekker, *Nature* **393**, 49 (1998).
12. W. Hoenlein, F. Kreupl, G. S. Duesberg, A. P. Graham, M. Liebau, R. Seidel, and E. Unger, *Mater. Sci. & Eng. C* **23**, 663 (2003).
13. H. L. Chang and C. T. Kuo, *Diamond Relat. Mater.* **10**, 1910 (2001).
14. Y. Saito and T. Yoshikawa, *J. Cryst. Growth* **134**, 154 (1993).
15. H. Murakami, M. Hirakawa, C. Tanaka, and H. Yamakawa, *Appl. Phys. Lett.* **76**, 1776 (2000).
16. D. C. Li, L. Dai, S. Huang, A. W. H. Mau, and Z. L. Wang, *Chem. Phys. Lett.* **316**, 349 (2000).
17. D. Zhou and S. Seraphin, *Chem. Phys. Lett.* **238**, 286 (1995).
18. M. Endo, S. Iijima, and M. S. Dresselhays(Eds.) *Carbon Nanotubes*, BPC Press, UK, pp. 37, 159 (1999).
19. C. H. Lin, H. L. Chang, C. M. Jsu, A. Y. Lo, and C. T. Kuo, *Diamond Relat. Mater.* **12**, 1851 (2003).
20. H. L. Chang, J. S. Fang, and C. T. Kuo, *Rev. Adv. Mater. Sci.* **5**, 432 (2003).
21. M. K. Sunkara, S. Shama, and R. Miranda, *Appl. Phys. Lett.* **79**, 1546 (2001).
22. C. A. Spindt, I. Brodie, I. Humphery, and E. R. Westerberg, *J. Appl. Phys.* **47**, 5248 (1976).